Emergency Voltage Regulation in Power Systems via Ripple-Type Control

Preprint

Guido Cavraro,[1] Manish K. Singh,[2] and Andrey Bernstein[1]

1 National Renewable Energy Laboratory
2 Virginia Tech

To be presented at the 29th Mediterranean Conference on Control and Automation (MED 2021)
June 22–25, 2021

NREL is a national laboratory of the U.S. Department of Energy
Office of Energy Efficiency & Renewable Energy
Operated by the Alliance for Sustainable Energy, LLC

This report is available at no cost from the National Renewable Energy Laboratory (NREL) at www.nrel.gov/publications.

Contract No. DE-AC36-08GO28308

Conference Paper
NREL/CP-5D00-79668
April 2021

Emergency Voltage Regulation in Power Systems via Ripple-Type Control

Preprint

Guido Cavraro,[1] Manish K. Singh,[2] and Andrey Bernstein[1]

1 National Renewable Energy Laboratory
2 Virginia Tech

Suggested Citation
Cavraro, Guido, Manish K. Singh, and Andrey Bernstein. 2021. *Emergency Voltage Regulation in Power Systems via Ripple-Type Control: Preprint*. Golden, CO: National Renewable Energy Laboratory. NREL/CP-5D00-79668.
https://www.nrel.gov/docs/fy21osti/79668.pdf.

NREL is a national laboratory of the U.S. Department of Energy
Office of Energy Efficiency & Renewable Energy
Operated by the Alliance for Sustainable Energy, LLC

This report is available at no cost from the National Renewable Energy Laboratory (NREL) at www.nrel.gov/publications.

Contract No. DE-AC36-08GO28308

Conference Paper
NREL/CP-5D00-79668
April 2021

National Renewable Energy Laboratory
15013 Denver West Parkway
Golden, CO 80401
303-275-3000 • www.nrel.gov

NOTICE

This work was authored in part by the National Renewable Energy Laboratory, operated by Alliance for Sustainable Energy, LLC, for the U.S. Department of Energy (DOE) under Contract No. DE-AC36-08GO28308. Funding provided by the Laboratory Directed Research and Development (LDRD) Program at NREL. The views expressed herein do not necessarily represent the views of the DOE or the U.S. Government.

This report is available at no cost from the National Renewable Energy Laboratory (NREL) at www.nrel.gov/publications.

U.S. Department of Energy (DOE) reports produced after 1991 and a growing number of pre-1991 documents are available free via www.OSTI.gov.

Cover Photos by Dennis Schroeder: (clockwise, left to right) NREL 51934, NREL 45897, NREL 42160, NREL 45891, NREL 48097, NREL 46526.

NREL prints on paper that contains recycled content.

Emergency Voltage Regulation in Power Systems via Ripple-Type Control

Guido Cavraro, Manish K. Singh, and Andrey Bernstein

***Abstract*— With increasing penetrations of volatile renewable generation and cyber-physical disruptions, ensuring the safe operation of bulk power systems has become unprecedentedly challenging. Because communication and computational costs restrict centralized system dispatch to being called upon every few minutes, and because purely local schemes are shown to be insufficient, distributed controls have been advocated for handling unanticipated system conditions in real time. The applicability of distributed control schemes, however, is fundamentally limited by their need for widespread communication and model cognizance. In this context, we put forth a hybrid, low-communication, saturation-driven protocol for the coordination of control agents that are distributed over a physical system and are allowed to communicate with peers over a "hotline" communication network. Under this protocol, when agents observe a constraint violation based on local measurements, they respond locally until their control resources saturate, in which case they send a beacon for assistance to peer agents. The scheme ensures that minor violations are efficiently mitigated via fast local controls, whereas severe violations can be handled by collaboration among a relatively small set of agents. We evaluate the performance of this scheme via numerical tests on the IEEE 14-bus test feeder, where agents act upon noisy measurements under diverse scenarios of load variations and severe low-/high-voltage events.**

I. Introduction

Power transmission networks were traditionally operated by centralized dispatchers, mainly by using bulk generation units to satisfy fairly predictable demands; however, network management is becoming formidably challenging due to rapid developments in policy and technology. For instance, the global push toward deregulation and data privacy calls for distributed privacy-preserving system operation. Moreover, increasing penetrations of distributed energy resources and flexible loads result in increased system volatility. Amidst these challenges, increasing occurrences of natural disasters and other critical cyber and physical disruptions undermine the stable and efficient operation of power systems. Bulk power systems are managed by system operators who aim to satisfy consumer demands in a cost-effective manner while meeting the related operational and physical constraints. Such tasks constitute the family of optimal dispatch problems (ODP). Consider a networked system modeled by an undirected graph $\mathcal{G} = (\mathcal{N}, \mathcal{E})$. The node set $\mathcal{N}$ with cardinality N hosts controllable agents, and vector $\mathbf{u} \in \mathbb{R}^N$ represents their *control inputs*. Often it is desired to regulate certain nodal variables within a desired range; thus, consider a subset of agents $\mathcal{Y} \subset \mathcal{N}$ of cardinality M that take local observations, which are stacked in vector $\mathbf{y} \in \mathbb{R}^M$. The entries of $\mathbf{y}$, henceforth referred to as *outputs*, are to be regulated within a desired range. We assume that given an input $\mathbf{u}$, the system has a locally unique output $\mathbf{y}$, determined by a mapping $\mathrm{F} : \mathbb{R}^N \to \mathbb{R}^M$. Heed that the mapping F might not necessarily have an explicit form and might be time varying. Network operators manage the respective systems by periodically computing the control set points that agents should implement. Usually, the control set points for time t are the solution of an ODP of the form:

$$\mathbf{u}^* \in \arg\min_{\mathbf{u}} \quad c(\mathbf{u}, \mathbf{y}) \tag{P1}$$

$$\text{s.to} \quad \mathbf{y} = \mathrm{F}(\mathbf{u}) \tag{1a}$$

$$\mathbf{h}(\mathbf{u}, \mathbf{y}) \leq \mathbf{0}, \tag{1b}$$

$$\underline{\mathbf{u}} \leq \mathbf{u} \leq \overline{\mathbf{u}} \tag{1c}$$

$$\underline{\mathbf{y}} \leq \mathbf{y} \leq \overline{\mathbf{y}} \tag{1d}$$

where $c(\mathbf{u}, \mathbf{y})$ is a function that could depend on the inputs and outputs of the system; the mapping in (1a) corresponds to the physical laws governing the network operation, whereas inequality constraints can be divided into two categories:

1) The constraint in (1b) incorporates requirements that might be important for efficient system operation but can in principle be safely violated (particularly for a brief time interval). We refer to these as *soft constraints*.

2) Constraints (1c) and (1d) impose limitations on input and output variables, respectively. The constraints on inputs are imposed by physical limitations, such as equipment rated capacity. The limits on output are often imposed by the operational, regulatory, or security requirements that must be satisfied at all times; therefore, these are referred to as *hard constraints*.

Typically, a network operator would solve ODPs at regular intervals based on anticipated demands and network conditions. Although ODP solutions might be able to ensure reliable system operation during normal conditions, their efficacy is limited during occurrences of unanticipated extreme disruptions that might undermine system operation; thus, to enhance resilience to these events, emergency control schemes are required that can operate in real time toward preventing system collapse.

This paper focuses on the design of emergency control

Manish K. Singh is with the Bradley Department of ECE, Virginia Tech, Blacksburg, VA 24061 USA (e-mail:{manishks, kekatos}@vt.edu). G. Cavraro and A. Bernstein are with the Power Systems Engineering Center, National Renewable Energy Laboratory, Golden, CO 80401 USA (e-mail: name.surname@nrel.gov). This work was authored in part by the National Renewable Energy Laboratory, operated by Alliance for Sustainable Energy, LLC, for the U.S. Department of Energy (DOE) under Contract No. DE-AC36-08GO28308. Funding provided by the NREL Laboratory Directed Research and Development Program. The views expressed in the article do not necessarily represent the views of the DOE or the U.S. Government. The U.S. Government retains and the publisher, by accepting the article for publication, acknowledges that the U.S. Government retains a nonexclusive, paid-up, irrevocable, worldwide license to publish or reproduce the published form of this work, or allow others to do so, for U.S. Government purposes.

This report is available at no cost from the National Renewable Energy Laboratory at www.nrel.gov/publications.

mechanisms that can ensure the satisfaction of system operational requirements during the time interval between two ODP actions. We refer to the proposed strategy as *ripple-type control*. It draws features from local, distributed, and event-triggered control. In local control rules, agents take decisions based on locally available measurements. For example, in [1], [2], power generators control their reactive power output given their local power injection and voltage; however, local schemes have limited efficacy [3]. To overcome such limitations while avoiding computationally expensive centralized interventions, distributed control strategies have been widely proposed. In such schemes, agents compute their control action after sharing information with neighbors on a communication network [4]. For instance, reference [5] proposes a primal-dual feedback approach in which every constraint violation results in the corresponding Lagrange multipliers being nonzero. Given that the inverter power outputs depend on all the Lagrange multipliers, in an event of a constraint violation, it's possible that all the agents in the network participate in corrective actions. Further, such schemes require widespread, frequent communication to update the values of the Lagrange multipliers. To avoid wasting resources and to communicate only when it is needed, event-triggered control techniques have been advocated in [6], [7]. Every agent locally evaluates a *triggering function*, e.g., in a consensus setup, the mismatch between the current state and the state that was last sent to neighbors [8]. When the triggering function takes some specified values, agents communicate and update their control rule.

Contrary to the previous approaches, in the proposed ripple-type control, agents first try to satisfy their local constraints via purely local control. Only when the local control efforts are saturated to their limits, assistance is sought from neighboring agents on a communication graph. The process is continued until all agents satisfy their local constraints. The proposed algorithm does not require knowledge of the system model parameters, and hence it is particularly suitable for real-time emergency control settings, wherein accurate model information is not readily available. In this paper, we extend the algorithm originally proposed in [9]. Further, we provide more extensive numerical tests investigating the performance of the proposed controller acting upon noisy measurements under diverse scenarios of random load variations and severe low-/high-voltage events.

Notation: Lower- (upper-) case boldface letters denote column vectors (matrices). Sets are represented by calligraphic symbols. Symbol $^\top$ stands for transposition. All-zero and all-one vectors are represented by $\mathbf{0}$ and $\mathbf{1}$; the respective dimensions are deducible from context. The $\mathrm{dg}(\cdot)$ operator places a vector on the principal diagonal of a matrix.

II. System Modeling

A power system is modeled by an undirected graph $\mathcal{G} = (\mathcal{N}, \mathcal{E})$. Nodes in the set $\mathcal{N}$, of cardinality N, are associated with electrical buses. For each bus n, denote its:

- Voltage magnitude and angle as $(v_n,\ \theta_n)$;
- The active and reactive power injection as $(p_n,\ q_n)$;

and collect the aforementioned quantities in the vectors $\mathbf{v}, \boldsymbol{\theta}, \mathbf{p}, \mathbf{q} \in \mathbb{R}^N$. A positive active (reactive) power means that active (reactive) power is *produced*, whereas a negative active (reactive) power means that active (reactive) power is *absorbed*. In a power network, usually a node is modeled as:

- A PQ bus whose active and reactive power injections are fixed at a known set point;
- A PV bus that controls its active power injection and voltage magnitude to a given set point;
- A slack bus able to set its voltage magnitude and angle.

For each of these bus types, having fixed two variables from $(v_n,\ \theta_n,\ p_n,\ q_n)$, the remaining are determined by the power flow equations. Loads are classically described as PQ buses absorbing a fixed amount of active and reactive power, generators as PV buses, and finally the biggest generator as the slack bus. The goal of the slack bus is to provide for any power deficit in the overall network at all times.

Edges in $\mathcal{E}$ are associated with power lines. Transmission lines are often approximated as lossless because their resistance is much smaller than their reactance; thus, ignoring line resistance, denote the admittance for line $\ell = (m, n)$ by $-jb_{mn}$, with $b_{mn} > 0$. The full AC power flow equations describe the relation between the nodal voltages and power injections; however, appending the lossless approximation with an assumption of small voltage angle differences across neighboring buses decouples the power flow equations into separate $\mathbf{p} - \boldsymbol{\theta}$ and $\mathbf{q} - \mathbf{v}$ systems. Therefore, voltage magnitudes can be approximated as a function of only reactive power injections. Because our goal is to develop an algorithm for voltage control, we focus on the $\mathbf{q} - \mathbf{v}$ model [10]:

$$\mathbf{q} = \mathrm{dg}(\mathbf{v})\mathbf{B}\mathbf{v}. \tag{2}$$

where matrix $\mathbf{B} \in \mathbb{R}^{N\times N}$ is a Laplacian matrix with line susceptances as weights. Specifically, it is defined as:

$$[\mathbf{B}]_{mn} = \begin{cases} -b_{mn}, & n \neq m \\ \sum_{k\neq n} b_{kn}, & n = m. \end{cases}$$

Partition the node set $\mathcal{N}$ into generator buses (both PV buses and the slack bus) and load buses as $\mathcal{N} = \mathcal{N}_G \oplus \mathcal{N}_L$, where the cardinality of $\mathcal{N}_G$ and $\mathcal{N}_L$ is G and L, respectively. Accordingly, partition vectors $(\mathbf{v}\ \mathbf{q})$ and matrix $\mathbf{B}$ as:

$$\mathbf{v} = \begin{bmatrix} \mathbf{v}_G \\ \mathbf{v}_L \end{bmatrix}, \mathbf{q} = \begin{bmatrix} \mathbf{q}_G \\ \mathbf{q}_L \end{bmatrix}, \mathbf{B} = \begin{bmatrix} \mathbf{B}_{GG} & \mathbf{B}_{GL} \\ \mathbf{B}_{LG} & \mathbf{B}_{LL} \end{bmatrix}$$

with $\mathbf{v}_G, \mathbf{q}_G \in \mathbb{R}^G$, $\mathbf{v}_L, \mathbf{q}_L \in \mathbb{R}^L$, $\mathbf{B}_{GG} \in \mathbb{R}^{G\times G}$, $\mathbf{B}_{LL} \in \mathbb{R}^{L\times L}$, $\mathbf{B}_{GL} = \mathbf{B}_{LG}^\top \in \mathbb{R}^{G\times L}$. Equation (2) becomes:

$$\begin{bmatrix} \mathbf{q}_G \\ \mathbf{q}_L \end{bmatrix} = \begin{bmatrix} \mathrm{dg}(\mathbf{v}_G) & \mathbf{0} \\ \mathbf{0} & \mathrm{dg}(\mathbf{v}_L) \end{bmatrix} \begin{bmatrix} \mathbf{B}_{GG} & \mathbf{B}_{GL} \\ \mathbf{B}_{LG} & \mathbf{B}_{LL} \end{bmatrix} \begin{bmatrix} \mathbf{v}_G \\ \mathbf{v}_L \end{bmatrix}. \tag{3}$$

Assume that the agents at all nodes measure the respective bus voltage magnitude. Because the voltages at generator buses are directly controled, our goal is to maintain the load voltages $\mathbf{v}_L$ within the stipulated limits; thus, the output $\mathbf{y}$ for the voltage regulation application comprises load voltage measurements. To regulate the load voltages, we suppose control flexibility at all buses. Specifically, generators are able to directly control their output voltage, whereas loads could partially control their reactive injections by exploiting

This report is available at no cost from the National Renewable Energy Laboratory at www.nrel.gov/publications.

inverters, capacitor banks, and flexible AC transmission systems; thus, depending on the bus type, the control variables for bus n are defined as:

$$u_n := \begin{cases} q_n & , \ n \in \mathcal{N}_L \\ v_n & , \ n \in \mathcal{N}_G \end{cases}$$

and are collected in the control vector $\mathbf{u} \in \mathbb{R}^N$. Given the control input $(\mathbf{q}_L, \ \mathbf{v}_G)$, output $\mathbf{v}_L$ is determined from the second block equation of (3) as an implicit relation. Generally, load voltages do not admit an explicit expression of the form $\mathbf{v}_L(\mathbf{u}) : \mathbb{R}^N \to \mathbb{R}^L$. Nevertheless, in later developing our voltage control algorithm, we will rely on the following *monotonicity assumption*

Assumption 1. *The load voltages are nondecreasing in the control inputs, that is:*

$$\frac{\partial v_n}{\partial u_m} \geq 0, \quad n \in \mathcal{N}_L, \, m \in \mathcal{N}$$

Assumption 1 essentially implies that the load voltages may be increased (decreased) by increasing (decreasing) the control inputs. Although such a monotonic assumption might seem simplistic at the outset, the next result provides a sufficient condition for Assumption 1 to hold.

Proposition 1. *Assumption 1 is satisfied if* $\mathrm{dg}(\mathbf{g}_L) + \mathbf{B}_{LL} \succ 0$ *where* $\mathbf{g}_L := [\mathrm{dg}(\mathbf{v}_L)]^{-2} \mathbf{q}_L$.

Proof. Adopting the implicit differentiation approach, apply the differential operator on the second block of (3):

$$\partial \mathbf{q}_L = (\mathrm{dg}(\mathbf{i}_L) + \mathrm{dg}(\mathbf{v}_L)\mathbf{B}_{LL}) \, \partial \mathbf{v}_L + \mathrm{dg}(\mathbf{v}_L)\mathbf{B}_{LG} \, \partial \mathbf{v}_G \tag{4}$$

where $\mathbf{i}_L := \mathbf{B}_{LG}\mathbf{v}_G + \mathbf{B}_{LL}\mathbf{v}_L$. Because $(\mathbf{q}_L, \mathbf{v}_G)$ are independent, it holds $\nabla_{\mathbf{q}_L} \mathbf{v}_G = \mathbf{0}$ so that (4) yields:

$$\nabla_{\mathbf{q}_L} \mathbf{v}_L = (\mathrm{dg}(\mathbf{i}_L) + \mathrm{dg}(\mathbf{v}_L)\mathbf{B}_{LL})^{-1}. \tag{5}$$

And because $\nabla_{\mathbf{v}_G} \mathbf{q}_L = \mathbf{0}$, equation (4) also provides:

$$\nabla_{\mathbf{v}_G} \mathbf{v}_L = -\left(\mathrm{dg}(\mathbf{i}_L) + \mathrm{dg}(\mathbf{v}_L)\mathbf{B}_{LL}\right)^{-1} \mathrm{dg}(\mathbf{v}_L)\mathbf{B}_{LG}. \tag{6}$$

For the Jacobian matrices $\nabla_{\mathbf{q}_L} \mathbf{v}_L$ and $\nabla_{\mathbf{v}_G} \mathbf{v}_L$ to have nonnegative entries, it suffices to show that the inverse of $\mathbf{G} := \mathrm{dg}(\mathbf{i}_L) + \mathrm{dg}(\mathbf{v}_L)\mathbf{B}_{LL}$ has nonnegative entries. This is because $\mathbf{v}_L > \mathbf{0}$ and $\mathbf{B}_{LG} \leq \mathbf{0}$.

To establish $\mathbf{G}^{-1} \geq \mathbf{0}$, note that the off-diagonal entries of $\mathbf{G}$ are nonpositive; hence, proving $\mathbf{G} \succ 0$ would make $\mathbf{G}$ an M-matrix so that $\mathbf{G}^{-1} \leq \mathbf{0}$. The assumption $\mathrm{dg}(\mathbf{g}_L) + \mathbf{B}_{LL} \succ 0$ stated in this proposition ensures $\mathbf{G} \succ 0$, as we show next. From (4), it follows that $\mathbf{q}_L = \mathrm{dg}(\mathbf{v}_L)\mathbf{i}_L$. Substituting $\mathbf{i}_L = \mathrm{dg}(\mathbf{v}_L)^{-1}\mathbf{q}_L$ in the stated condition yields:

$$\begin{aligned} &\mathrm{dg}(\mathbf{i}_L)\,\mathrm{dg}(\mathbf{v}_L)^{-1} + \mathbf{B}_{LL} \succ 0 \implies \\ &\mathrm{dg}(\mathbf{i}_L) + \mathrm{dg}(\mathbf{v}_L)^{1/2}\mathbf{B}_{LL}\,\mathrm{dg}(\mathbf{v}_L)^{1/2} \succ 0 \implies \\ &\mathrm{dg}(\mathbf{i}_L) + \mathrm{dg}(\mathbf{v}_L)\mathbf{B}_{LL} = \mathbf{G} \succ 0 \end{aligned}$$

where the first transition follows from Sylvester's law of inertia for congruent matrices, and the second follows from the similarity transformation involved. □

Proposition 1 shows that Assumption 1 holds for the grid model in (2) under the identified conditions. Numerically verifying $\mathrm{dg}(\mathbf{g}_L) + \mathbf{B}_{LL} \succ 0$ for real-world systems led us to an interesting observation, described next. For the IEEE 5-, 39-, and 118-bus systems, we scaled up the nominal $\mathbf{q}_L$ by a scalar until the power flow solver MATPOWER [11] failed to converge. At every step, we also observed the minimum eigenvalue of $\mathrm{dg}(\mathbf{g}_L) + \mathbf{B}_{LL}$. Interestingly, the minimum eigenvalue kept decreasing for increasing $\mathbf{q}_L$ but remained positive until the last successful power flow instance for all networks. This indicates a relation between $\mathrm{dg}(\mathbf{g}_L) + \mathbf{B}_{LL} \succ 0$ and the solvability of the AC power flow equations, but its analytical investigation goes beyond the scope of this work.

III. Ripple-Type Network Control

Transmission system operators' rendition of (P1) is often referred to as an optimal power flow (OPF) problem. A typical OPF formulation can be mapped to (P1) as follows:

- The function to be minimized $c(\mathbf{u}, \mathbf{y})$ usually models the power generation cost or the power losses [12];
- Constraint (1a) represents the power flow equations;
- The inequality (1b) models soft constraints, which are relatively less time-sensitive, for instance, line flow limits;
- Constraint (1c) models limits on generator output voltages and available load power flexibility;
- Inequality (1d) models load voltage constraints that could lead to instability if violated. These limits are typically modeled via box constraints as:

$$\underline{\mathbf{v}}_{\min} \leq \mathbf{v}_L \leq \overline{\mathbf{v}}_{\max}. \tag{7}$$

After solving (P1), given the mapping F, the system operator dispatches the optimal control set points $\mathbf{u}^*$ to agents. Ideally, this process shall be repeated every time there is a change in the system model that modifies the underlying definition of F, such as a load variation or a network topology change. Constrained by communication and computational resources, however, problem (P1) is solved only at finite time intervals. As a consequence, the set points $\mathbf{u}^*$ might become obsolete or even result in network constraint violations.

Such limitations motivate the design of mechanisms to at least ensure that critical operational requirements are met between two centralized dispatch actions, i.e., to make the control vector $\mathbf{u}$ belong to the security-focusing feasible set:

$$\mathcal{F} = \{\mathbf{u} : \ \underline{\mathbf{u}} \leq \mathbf{u} \leq \bar{\mathbf{u}}, \ \mathbf{v}_L = \mathrm{F}'(\mathbf{u}), \underline{\mathbf{v}}_{\min} \leq \mathbf{v}_L \leq \overline{\mathbf{v}}_{\max}\}$$

in which F' is the input-output mapping defined after a change in the system model. Set $\mathcal{F}$ considers only the hard constraints of (P1), namely, (1c) and (1d). The algorithm proposed next is designed to possess the ensuing key features:

F1) Prioritize local control: Agent $n \in \mathcal{Y}$ controls u_n locally based on a measurement of y_n. If the hard constraints (7) are violated, local control resources are used first.

F2) Communicate when saturated: Agent n transmits beacon signals to a few peer agents over a "hotline" communication network only if $u_n \in \{\underline{u}_n, \bar{u}_n\}$, i.e., only when local control resources reach their limits; and

This report is available at no cost from the National Renewable Energy Laboratory at www.nrel.gov/publications.

F3) Model-free: The control scheme is unaware of the model parameters, i.e., it is a model-free approach not requiring explicit knowledge of operator F'.

The communication network is modeled as an undirected graph $\mathcal{G}_c = (\mathcal{N}, \mathcal{E}_c)$. The topology of $\mathcal{G}_c$ is agnostic and unrelated of the power network graph $\mathcal{G}$; thus, the communication links $\mathcal{E}_c$ do not necessarily coincide with the transmission lines. As a consequence, the communication graph $\mathcal{G}_c$ remains unchanged during topology reconfigurations in the power network. Graph $\mathcal{G}_c$ is henceforth assumed to be connected, and denote its adjacency matrix as $\mathbf{A}$, where $A_{mn} = 1$ if there is a direct communication link between nodes m and n, i.e., $(m, n) \in \mathcal{E}_c$; and $A_{mn} = 0$ otherwise.

Next, let function $\mathbf{f} : \mathbb{R}^N \to \mathbb{R}^N_+$ denote a piecewise linear function quantifying the violation of constraint (1d) (or (7)). Specifically, function $\mathbf{f}(\cdot)$ is defined entry-wise as:

$$f_n(\mathbf{u}) := \begin{cases} \underline{y}_n - y_n(\mathbf{u}), & y_n(\mathbf{u}) \leq \underline{y}_n,\ n \in \mathcal{Y} \\ \overline{y}_n - y_n(\mathbf{u}), & y_n(\mathbf{u}) \geq \overline{y}_n,\ n \in \mathcal{Y} \\ 0, & y_n(\mathbf{u}) \in [\underline{y}_n, \overline{y}_n],\ n \in \mathcal{Y} \\ 0, & n \notin \mathcal{Y}. \end{cases} \tag{8}$$

Note that f_n zero when (1d) holds true, whereas it is positive (negative) if the lower (upper) constraint is violated. Further, it is zero-padded for buses not in $\mathcal{Y}$. Our control algorithm is reported next.

Ripple-Type Control for Voltage Regulation

Let $\mathbf{u}(0)$ be the initial control variables. Introduce the auxiliary variable $\boldsymbol{\lambda} \in \mathbb{R}^N$, and initialize it as $\boldsymbol{\lambda}(0) = \mathbf{0}$. For times $t \geq 1$:

1- Agents compute $\mathbf{f}(\mathbf{u}(t))$ according to (8).

2- A target set point is computed as:

$$\hat{\mathbf{u}}(t+1) = \mathbf{u}(t) + \mathrm{dg}(\boldsymbol{\eta}_1)\mathbf{f}(\mathbf{u}(t)) + \mathrm{dg}(\boldsymbol{\eta}_2)\mathbf{A}\boldsymbol{\lambda}(t) \tag{9}$$

for positive $\boldsymbol{\eta}_1$ and $\boldsymbol{\eta}_2$. Note that for node n, the target $\hat{u}_n(t)$ is computed using the local reading $y_n(t)$ and the entries of $\boldsymbol{\lambda}$ sent from its peers (neighbor nodes of node n on $\mathcal{G}_c$).

3- Agents compute the entries of the auxiliary vector $\boldsymbol{\lambda}$ as:

$$\lambda_n(t+1) = \begin{cases} \eta_{3,n}(\hat{u}_n(t+1) - \overline{u}_n), & \hat{u}_n(t+1) \geq \overline{u}_n \\ \eta_{3,n}(\hat{u}_n(t+1) - \underline{u}_n), & \hat{u}_n(t+1) \leq \underline{u}_n \\ 0, & \text{otherwise} \end{cases}, \tag{10}$$

for a positive constant $\boldsymbol{\eta}_3$. Vector $\boldsymbol{\lambda}$ serves as a beacon for assistance that is communicated across peer nodes.

4- The target set point is projected to the feasible range and physically implemented.

$$u_n(t+1) = \begin{cases} \overline{u}_n, & \hat{u}_n \geq \overline{u}_n \\ \underline{u}_n, & \hat{u}_n \leq \underline{u}_n \\ \hat{u}_n & \underline{u}_n \leq u_n \leq \overline{u}_n \end{cases} \tag{11}$$

The rationale behind the algorithm is the following. Suppose that load n is experiencing an overvoltage. Then, it starts decreasing its reactive power injection using its local flexibility. Because of the monotonicity of Assumption 1, this has the effect of decreasing v_n. At this point, there are two cases. First, load n is able to steer v_n within the desired limits in (7), and the corrective control actions end. Second, load n is not able to fix its voltage level because it depletes its control resources; therefore, λ_n becomes negative and is sent to the neighbors on the communication graph, which start decreasing their reactive power output, too. The process is repeated until (7) is met. Similar considerations can be done in the case in which load n is experiencing an undervoltage. The participation of various agents toward alleviating a voltage violation event propagates over neighboring nodes in a ripple-type manner, hence inspiring the name.

The novel control scheme satisfies feature *F1)* by design. Moreover, for a node n with target set points $\hat{u}_n(t+1)$ within the local control limit $\bar{u}_n$, the corresponding entry of $\boldsymbol{\lambda}(t+1)$ is zero; thus the computation of $\hat{u}_m$ from (9) for nodes m that are neighbors of n requires no communication from node n, hence fulfilling *F2)*. The scheme also meets *F3)* because it is agnostic to changes in topology and/or demands.

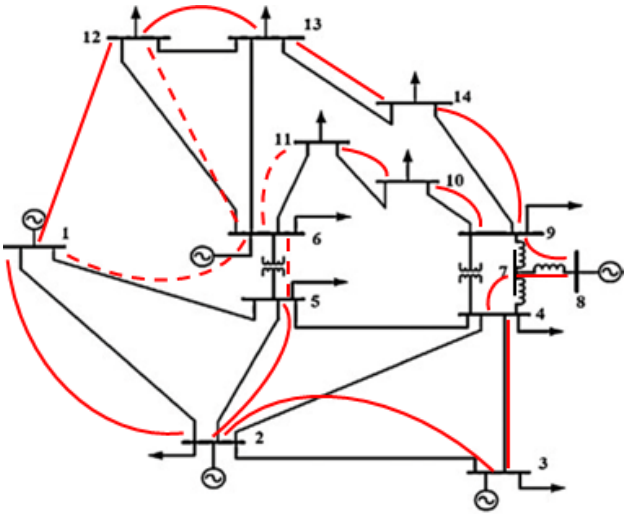

Fig. 1. The IEEE 14-bus test system. Red edges (both solid and dashed) represent communication links among buses. Dashed red edges are communication links that are broken after the major disruption at time $t = 24$ min.

IV. Numerical Tests

The ripple-type control scheme was tested on the IEEE 14-bus test feeder shown in Fig. 1. The red edges show the undirected communication graph over which the agents communicate. The generator at Bus 1 serves as the system slack bus with voltage set to 1 p.u. Each sensor introduces noise $e_n(t)$ that, for every time t, belongs to a Gaussian zero mean distribution with standard deviation of 10^{-2} [13]; namely, load n measures $y_n(t) = v_n(t) + e_n(t)$. The parameters for the developed scheme were numerically set to $\boldsymbol{\eta}_2 = 0.5 \cdot \mathbf{1}, \boldsymbol{\eta}_3 = \mathbf{1}$, whereas:

$$[\boldsymbol{\eta}_1]_n = \begin{cases} 0.01, & n \text{ is a generator} \\ 1, & n \text{ is a load} \end{cases}$$

The maximum and minimum voltages are set to $V_{\max} = 1.05$ p.u. and $V_{\min} = 0.95$ p.u., and $\underline{\mathbf{v}}_{\min} = V_{\min}\mathbf{1}, \underline{\mathbf{v}}_{\max} = V_{\max}\mathbf{1}$. The reactive power flexibility at the load buses is set to ± 2 MW with reference to their nominal values.

To comprehensively test and demonstrate the performance of the proposed control scheme under varying scenarios

This report is available at no cost from the National Renewable Energy Laboratory at www.nrel.gov/publications.

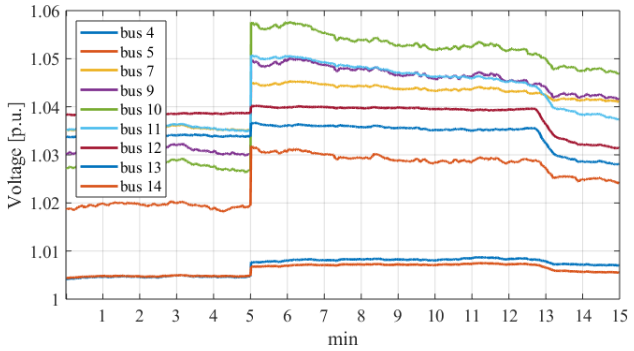

Fig. 2. At time $t = 5$ min, a fault at Bus 10 makes it abnormally increase its reactive power injections; hence, some voltages exceed $V_{\max}$

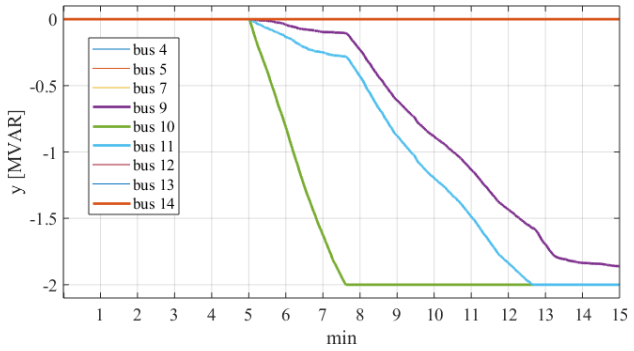

Fig. 3. Trajectories of the load bus-controled reactive power outputs. Load buses 9, 10, and 11 perform the ripple-type control. Bus 10 and Bus 11 saturate their reactive power output near time $t = 8$ and $t = 13$, respectively.

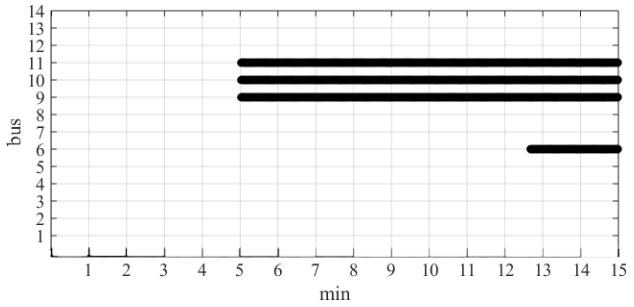

Fig. 4. The black lines cover the times when agents are performing the ripple-type control. Here, buses 9, 10, and 11 start changing their power injections at time $t = 5$ min, whereas Bus 6 intervenes near time $t = 13$.

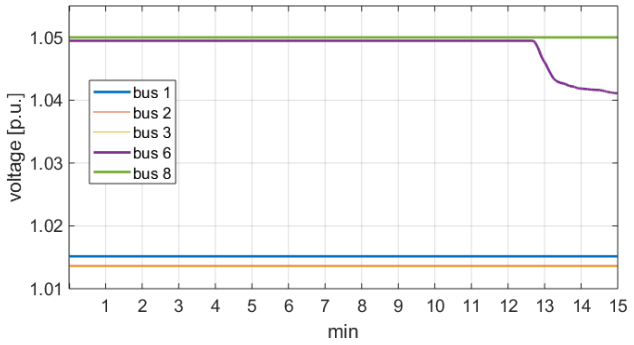

Fig. 5. Generator voltage magnitudes trajectories. Only the generator at Bus 6 participates in the ripple-type control.

of load variations and severe low-/high-voltage events, we performed a second-based simulation lasting for 30 min. Considering a typical centralized OPF dispatch interval of 15 min, our test witnesses three centralized dispatches of the form (P1) at $t = 0,\ 15$, and 30 min. During the overall 30-min duration, load variations, local measurements, and ripple control actions are assumed to be updated every second. The (re)active load variations are modeled as:

$$p_n(t+1) = p_n(t) + \delta_n^p(t)$$
$$q_n(t+1) = q_n(t) + \delta_n^q(t)$$

with $\delta_n^p(t), \delta_n^q(t)$ drawn from a zero-mean Gaussian distribution with a standard deviation of $0.68\bar{p}_n$ and $0.68\bar{q}_n$, respectively, where $\bar{p}_n$ and $\bar{q}_n$ are the nominal active and reactive power consumptions [14]. Next, we simulated two extreme events causing extreme high and low voltages, respectively.

At time $t = 0$, the optimal generator set points are computed and dispatched by the system operator. Thereafter, random load fluctuations translate to variations in load voltages; see Fig. 2. Despite small fluctuations, the voltages remain within the desired limits for the first 5 min. At $t = 5$ min, an abrupt increase in reactive power injection at Bus 10 is simulated. Such an event could be caused by a sudden capacitive load pickup or a faulty switching-in of a large capacitor bank. The simulated event results in an increased voltage causing overvoltages at buses 9, 10, and 11. Based on the local noisy measurements, the agents at buses 9, 10, and 11 start reducing their reactive power demands based on the ripple-type control; see Fig. 3. The involvement of various nodal agents in the ripple-type control is shown in Fig. 4. Initially, the agents at buses 9, 10, and 11 use their local flexibility and decrease their reactive demand. Fig. 3 shows that Bus 10 depletes its control resources near time $t = 8$ min. After that, it sends a beacon for assistance to its neighbors on the communication graph, namely, buses 9 and 11. Because they are already taking corrective actions, the number of active agents in Fig. 4 does not change; however, near time $t = 13$ min, Bus 11 depletes its control resources, too, and seeks help from its neighbors. Fig. 5 shows that near $t = 13$ min, Generator 6 starts to reduce its output voltage and subsequently reduces the load voltages to within the desired limits. Notably, only a few buses had to change their control inputs to successfully respond to the overvoltage event.

The second centralized OPF dispatch occurs at $t = 15$ min, accommodating all intra-dispatch load variations, and resetting the flexible deviations in load reactive power to zero; see Fig. 6. An extreme disruption is simulated at $t = 24$ min, causing a complete outage of generator Bus 6 and all the transmission and communication lines connected to it. As an immediate consequence, buses $11 - 14$ experience severe undervoltage conditions, potentially making the system vulnerable to voltage collapse. Thus, buses $11 - 14$ initially respond via local resources; see Fig. 6. Thereafter, other agents start collaborating via corrective actions for increasing the load voltages, subsequently succeeding near

This report is available at no cost from the National Renewable Energy Laboratory at www.nrel.gov/publications.

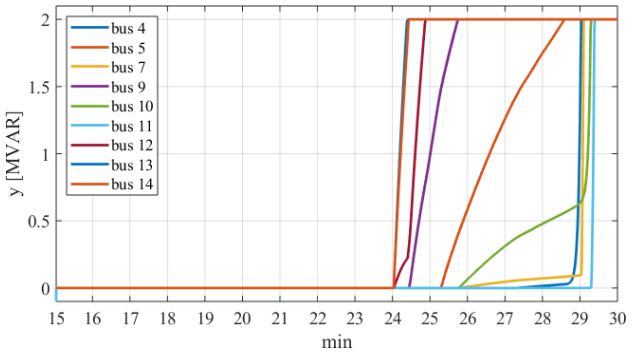

Fig. 6. Trajectories of the load bus-controled reactive power outputs.

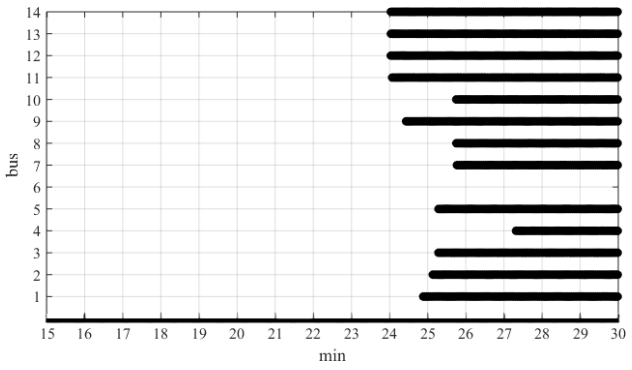

Fig. 7. The black lines cover the times when agents are performing the ripple-type control. First, buses 11, 12, 13, and 14 start changing their power injections at time $t = 24$ min. After that, sequentially, all the other buses take corrective actions, too.

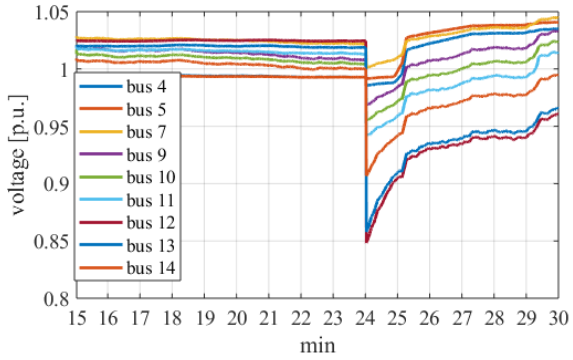

Fig. 8. At time $t = 24$ min, Bus 6 gets disconnected from the network, producing some undervoltage conditions.

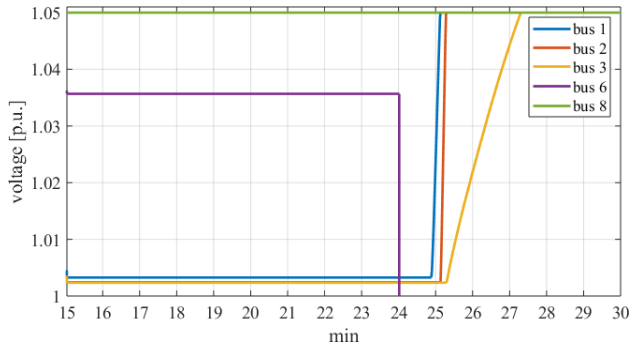

Fig. 9. Generator voltage magnitudes trajectories. Note that at time $t = 24$, the voltage at Generator 6 reduces to zero because of the outage.

$t = 29$ min; see Figs. 7, 8, and 9.

V. Conclusions

An emergency voltage control algorithm has been proposed. Generators and controllable loads act based on local control rules as long as local resources have not been depleted. When this happens, agents solicit help from neighbors in a communication network. The participation of various agents toward alleviating a voltage violation event propagates over neighboring nodes in a ripple-type manner. Elaborate numerical tests demonstrate that minor violations are efficiently tackled via fast local controls, whereas severe violations can be handled by collaboration among a relatively small set of agents; thus, the proposed algorithm is shown to elegantly combine the advantages of local and distributed controls, simultaneously foregoing the need for model cognizance. Future research will be focused on formally proving the stability of the control scheme and optimally deigning the communication graph.

References

[1] H. Zhu and H. J. Liu, "Fast local voltage control under limited reactive power: Optimality and stability analysis," *IEEE Trans. Power Syst.*, vol. 31, no. 5, pp. 3794–3803, Sep. 2016.

[2] X. Zhou, M. Farivar, Z. Liu, L. Chen, and S. Low, "Reverse and forward engineering of local voltage control in distribution networks," *IEEE Trans. Autom. Contr.*, pp. 1–1, May 2020.

[3] S. Bolognani, R. Carli, G. Cavraro, and S. Zampieri, "On the need for communication for voltage regulation of power distribution grids," *IEEE Trans. Control Netw. Syst.*, vol. 6, no. 3, pp. 1111–1123, Sep. 2019.

[4] D. K. Molzahn, F. Dörfler, H. Sandberg, S. H. Low, S. Chakrabarti, R. Baldick, and J. Lavaei, "A survey of distributed optimization and control algorithms for electric power systems," *IEEE Transactions on Smart Grid*, vol. 8, no. 6, pp. 2941–2962, 2017.

[5] C. Chang, M. Colombino, J. Cortés, and E. Dall'Anese, "Saddle-flow dynamics for distributed feedback-based optimization," *IEEE Contr. Syst. Lett.*, vol. 3, no. 4, pp. 948–953, Oct. 2019.

[6] W. P. M. H. Heemels, K. H. Johansson, and P. Tabuada, "An introduction to event-triggered and self-triggered control," in *Proc. IEEE Conf. on Decision and Control*, Maui, HI, Dec. 2012, pp. 3270–3285.

[7] S. Magnusson, C. Fischione, and N. Li, "Optimal voltage control using event triggered communication," in *Proc. 10th ACM Int. Conf. Future Energy Syst. (e-Energy)*, Phoenix, AZ, Jun. 2019, pp. 343–354.

[8] C. Nowzari and J. Cortés, "Distributed event-triggered coordination for average consensus on weight-balanced digraphs," *Automatica*, vol. 68, pp. 237–244, Jun. 2016.

[9] M. Singh, G. Cavraro, A. Bernstein, and V. Kekatos, "Ripple-type control for enhancing resilienceof networked physical systems," in *Proc. American Control Conf.*, New Orleans, LA, May 2021.

[10] J. W. Simpson-Porco, F. Dorfler, and F. Bullo, "Voltage stabilization in microgrids via quadratic droop control," *IEEE Trans. Autom. Contr.*, vol. 62, no. 3, pp. 1239–1253, Mar. 2017.

[11] R. D. Zimmerman, C. E. Murillo-Sanchez, and R. J. Thomas, "MATPOWER: steady-state operations, planning and analysis tools for power systems research and education," *IEEE Trans. Power Syst.*, vol. 26, no. 1, pp. 12–19, Feb. 2011.

[12] M. Huneault and F. D. Galiana, "A survey of the optimal power flow literature," *IEEE Transactions on Power Systems*, vol. 6, no. 2, pp. 762–770, 1991.

[13] J. Zhao, M. Netto, and L. Mili, "A robust iterated extended kalman filter for power system dynamic state estimation," *IEEE Transactions on Power Systems*, vol. 32, no. 4, pp. 3205–3216, 2017.

[14] G. Cavraro and R. Arghandeh, "Power distribution network topology detection with time-series signature verification method," *IEEE Transactions on Power Systems*, vol. 33, no. 4, pp. 3500–3509, 2018.

This report is available at no cost from the National Renewable Energy Laboratory at www.nrel.gov/publications.